I&EC research
Industrial & Engineering Chemistry Research

Article

Cite This: Ind. Eng. Chem. Res. 2019, 58, 11072−11081

pubs.acs.org/IECR

Solubility and Diffusivity of Chlorodifluoromethane in Imidazolium Ionic Liquids: [emim][Tf_2N], [bmim][BF_4], [bmim][PF_6], and [emim][TFES]

David L. Minnick[†] and Mark B. Shiflett[*]

Department of Chemical & Petroleum Engineering and Center for Environmentally Beneficial Catalysis, University of Kansas, Lawrence, Kansas 66045, United States

Supporting Information

ABSTRACT: Solubility and diffusivity measurements of chlorodifluoromethane (HCFC-22) in four ionic liquids (ILs)—[emim][Tf_2N], [bmim][BF_4], [bmim][PF_6], and [emim][TFES]—were conducted using an IGA gravimetric microbalance at temperatures between 283.2 and 348.2 K. The solubility results were modeled using the NRTL activity coefficient method and were also used to calculate Henry's law constants (k_H) at infinite dilution. van't Hoff relationships were used to calculate the enthalpy ($\Delta\bar{H}_{sol}$) and entropy ($\Delta\bar{S}_{sol}$) of absorption for HCFC-22 in each IL. Time-dependent absorption data collected by the IGA microbalance was used to calculate the diffusion coefficient of HCFC-22 in each IL. The diffusion coefficient results were used to calculate the hydrodynamic radius of the solute molecule using the Stokes−Einstein relationship. The experimental results for chlorodifluoromethane and [emim][Tf_2N] are compared with previous studies on trifluoromethane and other fluorocarbons to understand the impact of atom substitution (e.g., CHF_2-F vs CHF_2-Cl) on fluorocarbon solubility in an ionic liquid.

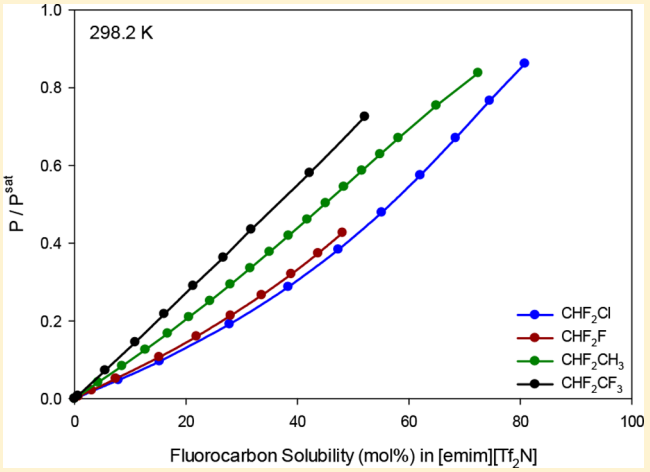

1. INTRODUCTION

Hydrochlorofluorocarbon (HCFC) refrigerants (e.g., chlorodifluoromethane, HCFC-22) were developed as environmentally friendly replacements for chlorofluorocarbons (CFCs) (e.g., dichlorodifluoromethane, CFC-12), which are linked to the depletion of the Earth's ozone layer. Despite their minimal ozone depletion potential (ODP) (e.g., HCFC-22 ODP = 0.05 compared with CFC-12 ODP = 1.0) and improved environmental properties, HCFC refrigerants are currently being phased out under the Montreal Protocol due to their ODP and high global warming potentials (GWP).[1] An initial strategy to develop increasingly environmentally friendly drop-in replacements for CFC refrigerants was to blend HCFC and hydrofluorocarbon (HFC) refrigerant gases (e.g., R-401a: 53 wt % HCFC-22, 34 wt % HCFC-124, 13 wt % HFC-152a). However, refrigerant gas blends using HCFCs are also currently being phased out as improved hydrofluorocarbon and hydrofluoroolefin (HFO) blends are developed. Despite its reduced use as a refrigerant gas, HCFC-22 remains an industrially important chemical as a precursor for the production of tetrafluoroethylene (TFE), which is used in the manufacturing of Teflon (polytetrafluoroethylene, PTFE). As HCFCs are continually phased out, being able to separate, recover, and purify individual components in refrigerant gas blends will become important.

Ionic liquids possess negligible volatility due to their ionic character and are therefore ideal absorbents for gas separations. Development of a gas separation process requires a thorough understanding of the sorbate−absorbent phase behavior. Shiflett and co-workers previously investigated the phase behavior of more than 20 HFC and HCFC compounds with ionic liquids,[2−11] which have led to separation schemes for select refrigerant gases, such as difluoromethane (HFC-32) and pentafluoroethane (HFC-125).[2,12,13] Here we continue these investigations by studying the solubility and diffusivity of chlorodifluoromethane in four ILs, including 1-ethyl-3-methylimidazolium bis(trifluoromethylsulfonyl)imide ([emim][Tf_2N]), 1-butyl-3-methylimidazolium tetrafluoroborate ([bmim][BF_4]), 1-butyl-3-methylimidazolium hexafluorophosphate ([bmim][PF_6]), and 1-ethyl-3-methylimidazolium 1,1,1,2-tetrafluoroethanesulfonate ([emim][TFES]). The experimental results for chlorodifluoromethane and [emim]-

Received: May 2, 2019
Revised: May 28, 2019
Accepted: May 31, 2019
Published: May 31, 2019

DOI: 10.1021/acs.iecr.9b02419
Ind. Eng. Chem. Res. 2019, 58, 11072−11081

[Tf_2N] at 298.2 K have been compared with previous studies on trifluoromethane and other fluorocarbon gases to understand the impact of atom substitution (CHF_2-*F* vs CHF_2-*Cl*) on refrigerant gas solubility in an IL.

2. MATERIALS AND METHODS

2.1. Materials. Chlorodifluoromethane (HCFC-22) was obtained from DuPont and was used as received. Ionic liquids were purchased from commercial suppliers as follows: [emim][Tf_2N] and [emim][TFES] were purchased from IoLiTec Gmbh, [bmim][PF_6] was purchased from Sigma-Aldrich, and [bmim][BF_4] was purchased from Fluka. The purity and lot number of each component is specified in Table 1.

Table 1. Chemical Component Properties

component	CAS number	purity (mol %)	source	lot number
HCFC-22	75-45-6	99	DuPont	
[emim][Tf_2N]	174899-82-2	99	IoLiTec	H00620.1
[emim][TFES]	880084-63-9	99	IoLiTec	I00113.1.3
[bmim][PF_6]	174501-64-5	≥98.5	Sigma-Aldrich	0001423194
[bmim][BF_4]	174501-65-6	≥98.5	Fluka	1291367

2.2. Experimental Methods. *2.2.1. Hiden IGA Microbalance.* Solubility measurements were experimentally conducted using a Hiden Intelligent Gravimetric Analyzer (IGA). The Hiden IGA microbalance was recently reviewed by our group and consists of a Pyrex sample cup and a 316 stainless steel counterweight that are oriented on opposite sides of a thermostatic balance beam.[14] The IGA microbalance is controlled by HISorp software, which allows solubility measurements to be obtained at precise pressures between vacuum (10^{-10} MPa) and 2 MPa and temperatures between 283.2 and 348.2 K, when configured with the Grant water bath attachment. The IGA microbalance is equipped with a Pfeiffer foreline and turbomolecular pump combination, allowing in situ pretreatment to be performed on the IL sample. Approximately 75 mg of IL was loaded into the Pyrex sample cup and pretreated in the IGA microbalance at ~10^{-10} MPa and 348.2 K for 24 h prior to each experiment to remove volatile impurities, including water. Water content in each IL is estimated to be less than 25 ppm after in situ pretreatment. This estimation was validated by pulling a comparable vacuum on select IL samples using a Schlenk line and then analyzing them using a coulometric Karl Fisher titration method. Sorption and desorption measurements were conducted with the microbalance configured in "static" mode. In this configuration, gas was admitted into the balance at a rate of 0.01 MPa/min until the set point was achieved. The admit and exhaust stepper motors then regulated the system pressure within ±0.00001 MPa throughout the experiment. A minimum of 3 h was provided for the sample to reach phase equilibrium in the IGA at each temperature and pressure point. The kinetic sorption profile and balance stability were monitored by the HISorp software program, which ensured that a stable equilibrium was achieved before acquiring a data point.

Pressure (P) and temperature (T) transducers in the IGA microbalance were calibrated using NIST certified reference instruments. IGA system pressure was measured by a Druck (model PDCR4010) pressure transducer, which had an operating range between vacuum and 2 MPa. The pressure transducer was calibrated against a NIST traceable Paroscientific model 765-1K pressure transducer (serial no. 101314), which has an accuracy of ±0.0008 MPa between vacuum and 6.89 MPa. Sample temperature was measured by a K-type thermocouple, which was calibrated against a NIST traceable standard platinum resistance thermometer (Hart Scientific SPRT model 5699 and readout Hart Scientific Blackstack model 1560 with a SPRT module 2560), which had an accuracy of ±0.005 K. The uncertainty of temperature and pressure in the IGA were within ±0.1 K and ±0.0008 MPa, respectively. The IGA balance has a mass resolution of ±0.1 μg and has an accuracy better than ±0.5 mol % (±0.1 mass %) for sorption experiments with ILs at any given T and P.

2.2.2. Force Balance Calculation. The internal IGA microbalance components are impacted by (i) aerodynamic drag forces, (ii) buoyant forces, (iii) balance sensitivity to temperature and pressure, and (iv) volume expansion of the liquid sample. Accurate gas solubility calculations require compensating for these factors by solving a force balance equation.

Sorption measurements were conducted with the balance in "static mode", where a controlled gaseous atmosphere was maintained in the balance using automated admit and exhaust valves to eliminate drag forces. The internal components of the IGA microbalance are impacted by their gaseous atmosphere according to Archimedes' principal, which states that the buoyant force applied to an object acts in an upward direction and is equivalent to the mass of the displaced fluid. A general equation used to compute the buoyant force (F_b) acting on an object is shown in eq 1, where (g) is gravitational acceleration, (V_i) is the volume of the object, and (ρ_g) is the density of the gas surrounding the object at a known temperature and pressure (T, P).

$$F_b = gV_i\rho_g = g\frac{m_i}{\rho_i}\rho_g(T,P) \tag{1}$$

Equation 2 is derived by applying the force balance equation to each component on the sample (i) and counterweight (j) sides of the balance:

$$\sum_{i=1} m_i - \sum_{j=1} m_j - \sum_{i=1}\frac{m_i}{\rho_i}\rho_g(T_i,P) + \sum_{j=1}\frac{m_j}{\rho_j}\rho_g(T_i,P) + m_s + m_a - \frac{m_s}{\rho_s(T_s)}\rho_g(T_i,P) - \frac{m_a}{\rho_a(T_a)}\rho_g(T_i,P) - C_f(T_s,P) = \text{balance reading} \tag{2}$$

where ($m_{i,j}$) is the balance component mass, ($\rho_{i,j}$) is the balance component density, (m_s) is sample mass, (ρ_s) is the sample density, (m_a) is the mass of the absorbed gas, and (ρ_a) is the density of the absorbed gas. Balance sensitivity to temperature and pressure is accounted for using a correction factor (C_f), which is measured by conducting an initial experiment at each temperature and pressure condition without the sample. Finally, volume expansion of the IL sample is accounted for using eq 3, where V_m is the mole fraction average of the pure component molar volumes.

$$\frac{m_s}{\rho_s(T_s)}\rho_g(T_s,P) + \frac{m_a}{\rho_a T_a}\rho_g = V_m(T,P)\,\rho_g(T,P) \tag{3}$$

Accurate mass and density values for each component of the instrument and sample are required. Mass and density

DOI: 10.1021/acs.iecr.9b02419
Ind. Eng. Chem. Res. 2019, 58, 11072−11081

properties of the IGA microbalance components were measured and provided by Hiden Isochema. Gas-phase density data was calculated using the National Institute of Standards and Testing (NIST) REFPROP v.9.1 database, which contains thermodynamic and transport properties for more than 80 compounds, including chlorodifluoromethane.[15] Liquid density properties of [emim][Tf_2N],[16] [bmim][BF_4],[17] [bmim][PF_6],[18] and [emim][TFES][19] were obtained from the literature. An increasingly detailed explanation of the buoyancy correction can be found in our recent review of gas sorption measurements using gravimetric microbalances.[14]

2.2.3. NRTL Activity Coefficient Modeling. The isothermal vapor−liquid equilibrium results were modeled using a so-called $\gamma-\phi$ method, where the liquid phase was modeled by the nonrandom two-liquid (NRTL) activity coefficient model and the vapor phase was modeled using a second virial coefficient correction. At low pressures the vapor−liquid equilibrium can be described by

$$x_i\gamma_i P_i^{vap} = y_i P\phi_i \tag{4}$$

where x_i, γ_i, and P_i^{vap} are the liquid-phase mole fraction composition, activity coefficient, and vapor pressure, respectively, of the ith component. Additionally, y_i and ϕ_i are the vapor-phase mole fraction composition and the Poynting pressure correction of the ith component and P is the system pressure. The ILs used in this study have immeasurable vapor pressures $P_{IL}^{vap} \approx 0$. Therefore, it is reasonable to assume that the vapor-phase composition is solely HCFC-22 and that $y_{IL} = 0$. With the preceding assumptions, the $\gamma-\phi$ equation can be reduced as follows:

$$x_1\gamma_1 P_1^{vap} = y_1 P\phi_1 \tag{5}$$

Here the numbering convention used throughout this paper is established, where component 1 represents HCFC-22 and component 2 represents the ionic liquid.

The liquid-phase composition x_1 and system pressure P are experimentally measured using the IGA microbalance. The vapor-phase composition ($y_1 = 1$) is based on the nonvolatility of the IL. The liquid-phase HCFC-22 activity coefficient is calculated using the NRTL model

$$\ln\gamma_1 = x_2^2\left[\tau_{21}\left(\frac{G_{21}}{x_1 + x_1G_{21}}\right)^2 + \frac{\tau_{12}G_{12}}{(x_2 + x_1G_{12})^2}\right] \tag{6}$$

where G_{12} and G_{21} are defined by the binary interaction parameters (τ_{12} and τ_{21})

$$G_{12} \equiv \exp(-\alpha\tau_{12}) \quad \text{and} \quad G_{21} \equiv \exp(-\alpha\tau_{21}) \tag{7}$$

and where the nonrandomness factor α is assumed to be a constant with a specified value of 0.2.

Temperature-dependent binary interaction parameters were used to regress the experimental solubility data for each system using a least-squares method solved by minimizing the error (%AARD) in pressure, where

$$\tau_{12} = \tau_{12}^{(0)} + \frac{\tau_{12}^{(1)}}{T[K]} + \tau_{12}^{(2)}\ln(T[K]) \quad \text{and}$$

$$\tau_{21} = \tau_{21}^{(0)} + \frac{\tau_{21}^{(1)}}{T[K]} + \tau_{21}^{(2)}\ln(T[K]) \tag{8}$$

The Poynting correction (ϕ_1) for HCFC-22 is calculated using the temperature-dependent second virial coefficient of HCFC-22 (B_1), which is obtained using the NIST REFPROP v.9.1 software package[15]

$$\phi_1 = \exp\left[\frac{(B_1 - \tilde{V}_1)(P - P_1^{vap})}{RT}\right] \tag{9}$$

where $\tilde{V}_1$ is the saturated molar volume of HCFC-22 at the system temperature T, the calculation method of which has been previously described by our group,[14] and R is the universal gas constant.

The vapor pressure of HCFC-22 was calculated using the Antoine vapor pressure model shown in eq 10

$$\ln P_1^{vap} = A + \frac{B}{T + C} \tag{10}$$

where T [K], P_1^{vap} [bar], and the coefficients are $A = 4.36567$, $B = -947.577$, and $C = -14.964$.[20]

2.2.4. Henry's Law Analysis. Henry's law modeling was performed on the experimentally measured solubility data to study the intermolecular interactions between HCFC-22 and each IL. Equation 11 shows the fundamental relationship between the Henry's law constant k_H and the chemical potential

$$\mu_i^{\infty} = \mu_i^{\circ} + RT\ln k_H \tag{11}$$

where μ_i^{∞} is the chemical potential of the solute at infinite dilution ($P,T\rightarrow 0$) and μ_i° is the chemical potential of the pure gas species at the system temperature and a reference pressure of 1 atm. Equation 11 can be rearranged to solve for the Henry's law constant as shown in eq 12.

$$k_H = \exp\left[\frac{\mu_i^{\infty} - \mu_i^{\circ}}{RT}\right] \tag{12}$$

An ideal solution is characterized by noninteracting species, a phenomenon which is commonly observed in dilute mixtures. Under these conditions the infinite dilution chemical potential of the solute is equal to its reference chemical potential and $k_H = 1$. The Henry's law constant can also be expressed as a function of fugacity for nonideal mixtures, as shown in eq 13

$$k_H = \lim_{x_1\rightarrow 0}\frac{f_1^V(T,P,y_1)}{x_1} \approx \left(\frac{df_1^V}{dx_1}\right)_{x_1=0} \tag{13}$$

where f_1^V is the vapor-phase fugacity of pure HCFC-22, which can be calculated by an equation of state model. In this analysis, the NIST REFPROP v.9.1 software package was used to calculate the pure component fugacities of HCFC-22 using the Helmholtz equation of state.[15,21] The Henry's law constant−fugacity relationship in eq 13 was modeled using the second-order polynomial expansion, shown in eq 14

$$f_1^V\,[\text{MPa}] = a_0 + a_1x_1 + a_2x_1^2 \tag{14}$$

where the Henry's law constant k_H is represented by the a_1 term based on the definition of the derivative shown in eq 13.

The temperature dependence of the Henry's law constant at constant pressure is related to the differential latent heat of solution $\Delta\bar{H}_{sol}$, shown in eq 15.

DOI: 10.1021/acs.iecr.9b02419
Ind. Eng. Chem. Res. 2019, 58, 11072−11081

Table 2. Coefficients for the Viscosity Model Shown in eq 22

component	A_i	B_i (K)	C_i (K^{-1})	D_i (K^{-2})
HCFC-22[15]	−10.3968	463.625	2.1258×10^{-2}	-2.10458×10^{-5}
[emim][Tf2N][4]	−131.216	16999.1	3.6455×10^{-1}	-3.49193×10^{-4}
[bmim][BF4][4]	−149.99	20757.8	3.9158×10^{-1}	-3.55363×10^{-4}
[bmim][PF6][4]	−182.744	24992.4	4.8402×10^{-1}	-4.44780×10^{-4}
[emim][TFES][19]	−79.5243	12445.7	1.8957×10^{-1}	-1.60156×10^{-4}

$$\left(\frac{\mathrm{d}(\ln k_H)}{\mathrm{d}\left(\frac{1}{T}\right)}\right)_P = \frac{\bar{H}_1^{\circ}(T,1\ \mathrm{atm})_g - \bar{H}_1^{\infty}(T,1\ \mathrm{atm})_l}{RT^2} \equiv \frac{\Delta\bar{H}_{sol}}{R} \tag{15}$$

Similarly, the temperature dependence of the Henry's law constant at constant pressure is related to the differential entropy of solution $\Delta\bar{S}_{sol}$, as shown in eq 16.

$$\left(\frac{\mathrm{d}(\ln k_H)}{\mathrm{d}(\ln T)}\right)_P = \frac{-\Delta\bar{S}_{sol}}{R} \tag{16}$$

2.2.5. Diffusion Coefficient Analysis. Experimental mass, temperature, and pressure measurements were acquired by the IGA microbalance at 1-s intervals. Equation 17 was used to fit the kinetic mass vs time data and calculate the Fickian one-dimensional diffusion coefficient of HCFC-22 in each IL.

$$\langle C\rangle = C_s\left[1 - 2\left(1 - \frac{C_o}{C_s}\right)\sum_{n=0}^{\infty}\frac{\exp(-\lambda_n^2 Dt)}{L^2\lambda_n^2}\right] \tag{17}$$

Here D is the diffusion coefficient, $\lambda_n = [n + 0.5]\left[\frac{\pi}{L}\right]$, $\langle C\rangle$ is the average concentration of gas in the liquid mixture at a given T and P, C_o is the initial solute concentration in the liquid mixture, C_s is the solute concentration in the liquid mixture at saturation ($t\rightarrow\infty$), and L is the liquid depth of the liquid sample. Detailed derivations of the Fickian one-dimensional diffusion coefficient equations and boundary conditions have been previously discussed by our group.[14] A nonlinear regression algorithm programed in MATLAB was used to solve eq 17 and calculate the effective diffusivity values.

The diffusion coefficient is very sensitive to the depth of the liquid sample L which increases as a function of absorbed solute mass. For example, the volume expansion of [emim][Tf_2N] with HCFC-22 was measured using a volumetric viewcell. The results showed that the liquid sample expanded by 134% at 298.2 K and 0.890 MPa where the solubility of HCFC-22 was measured to be 81.8 mol %.[14] This result indicates that the volume expansion of the IL sample (i.e., change in sample height) is significant at certain *TPx* conditions.

The diffusion coefficient analysis in this study accounted for volume expansion of the liquid sample by calculating two diffusion coefficient values using the height of the solution at initial composition (C_o) and again using the height at the final saturated composition (C_s). The average of these values resulted in an effective diffusion coefficient value at each pressure. While volume expansion is a nonlinear phenomenon, over small pressure (e.g., 0.1 MPa) and solubility ranges, a linear approximation is sufficient.

2.2.6. Stokes−Einstein Modeling. The Stokes−Einstein correlation is used to model an ideal scenario where a spherical solute molecule moves through a quiescent fluid phase. The semitheoretical correlation, shown in eq 18, was applied to calculate the molecular radius of the diffusing gas species (HCFC-22) using the calculated gas diffusivity with an estimated solution viscosity.

$$D = \frac{k_B T}{6\pi r\eta_o(\eta/\eta_o)^b} \tag{18}$$

The linearized form of eq 18 is shown below

$$\ln\left(\frac{D}{T}\right) = a - b\ln\left(\frac{\eta}{\eta_o}\right) \tag{19}$$

where $a = \ln(k_b/6\pi r\eta_o)$ and b are adjustable parameters, k_b is the Boltzmann constant, r is the radius of the diffusing species, and η_o is the unit viscosity (1 MPa·s) for proper dimensional analysis.

Viscosity of the IL−refrigerant gas mixture was calculated using the previously derived model[22] shown in eq 20

$$\ln\left(\frac{\eta}{\eta_o}\right) = \sum_{i=1}^{N}\xi_i\ln\left(\frac{\eta_i}{\eta_o}\right) \tag{20}$$

where

$$\xi_i = \frac{M_i^c x_i}{\sum_{i=1}^{N} M_i^c x_i} \tag{21}$$

and M_i is the molecular weight of the ith species. The dynamic viscosity of each pure compound is modeled using previously published data[4,15,19] according to

$$\ln(\eta_i) = A_i + \frac{B_i}{T} + C_i T + D_i T^2 \tag{22}$$

where η_i is in units of cP and T is in units of K. Coefficients for the viscosity model for HCFC-22 and each of the ionic liquids are displayed in Table 2.

3. RESULTS AND DISCUSSION

3.1. IGA Method Validation. The performance of the IGA microbalance was validated by measuring the solubility of CO_2 in the IL [hmim][Tf_2N]. The experimental solubility results acquired by our group in 2018 were compared to those measured by Shiflett et al. in 2007, which were collected as part of an International Union of Pure and Applied Chemistry (IUPAC) study on the "Thermodynamics of Ionic Liquids, Ionic Liquid Mixtures, and the Development of Standard Test Systems".[23−26] Our recent [hmim][Tf_2N] + CO_2 solubility results agree within ±0.5 mol % of the results in the published IUPAC study, indicating the ability of the IGA method to accurately and reproducibly measure vapor−liquid equilibria data for IL + compressed gas systems similar to those investigated in this study.[14]

3.2. Vapor−Liquid Equilibrium and Thermodynamic Modeling Results. Isothermal solubility measurements *PTx* of HCFC-22 in a series of imidazolium ionic liquids were

DOI: 10.1021/acs.iecr.9b02419
Ind. Eng. Chem. Res. 2019, 58, 11072−11081

Table 3. Experimental Solubility (PTx) and Diffusivity (D) Data for HCFC-22 in [bmim][BF_4] and [bmim][PF_6]

(1) HCFC-22 + (2) [bmim][BF_4]				(1) HCFC-22 + (2) [bmim][PF_6]			
T (K)	P (MPa)	mol % ($100x_1$)	$D \times 10^{-11}$ (m^2/s)	T (K)	P (MPa)	mol % ($100x_1$)	$D \times 10^{-11}$ (m^2/s)
283.2	0.0500	10.2	3.1	283.2	0.0500	8.2	1.5
283.1	0.1000	20.0		283.2	0.1000	16.3	
283.2	0.2000	37.2		283.2	0.2000	32.1	
283.2	0.3000	50.9	53	283.2	0.3000	46.1	10
283.1	0.4000	62.3		283.2	0.4000	58.6	
283.1	0.5000	72.5		283.2	0.5000	69.9	
283.1	0.6000	82.7	77	283.2	0.6000	81.4	66
298.2	0.0500	6.3	7.5	298.2	0.0500	5.0	2.8
298.2	0.1000	12.4		298.2	0.1000	10.4	
298.2	0.2000	23.5		298.2	0.2000	20.7	
298.2	0.3000	33.5	31	298.2	0.3003	30.5	8.2
298.2	0.4000	42.3		298.2	0.4002	39.6	
298.2	0.5000	50.4		298.2	0.5002	48.0	
298.2	0.6000	57.6	95	298.2	0.6000	55.8	27
298.2	0.7000	64.2		298.2	0.7000	63.2	
298.2	0.8000	70.8		298.2	0.8000	70.4	
298.1	0.8994	78.6	160	298.2	0.9001	77.9	76
298.1	0.8994	78.6		298.2	0.9001	77.9	
298.2	0.8001	70.5		298.2	0.8000	70.4	
298.2	0.7000	63.1		298.1	0.7000	63.2	
298.2	0.5999	56.4		298.2	0.6005	55.8	
298.2	0.5000	49.5		298.2	0.5003	48.1	
298.2	0.4000	42.2		298.2	0.4001	39.8	
298.2	0.3000	34.3		298.2	0.3002	30.8	
298.2	0.2000	25.0		298.2	0.2003	21.3	
298.2	0.1000	14.1		298.1	0.1006	10.9	
298.2	0.0500	8.0		298.2	0.0503	5.3	
323.2	0.0500	3.1	15	323.2	0.0500	2.9	6.1
323.2	0.1000	6.3		323.2	0.1000	5.7	
323.2	0.2000	12.6		323.2	0.2000	11.2	
323.2	0.3000	18.6	28	323.2	0.3000	16.6	11
323.2	0.4000	24.4		323.2	0.4000	21.9	
323.2	0.5001	29.8		323.2	0.4996	27.0	
323.2	0.6000	34.9	50	323.2	0.6000	31.8	17
323.2	0.7000	39.7		323.2	0.7000	36.5	
323.2	0.8000	44.2		323.2	0.8000	40.9	
323.2	0.9000	48.4	78	323.2	0.8998	45.3	28
348.2	0.0500	1.7	20	348.2	0.0500	1.7	14
348.2	0.1000	3.6		348.2	0.1000	3.3	
348.1	0.2000	7.3		348.1	0.2000	6.5	
348.2	0.3000	10.8	36	348.2	0.3000	9.7	17
348.1	0.4000	14.2		348.2	0.4000	12.8	
348.2	0.5000	17.6		348.2	0.5000	16.0	
348.2	0.6000	20.9	42	348.2	0.6001	19.1	22
348.2	0.7000	24.1		348.1	0.7000	22.2	
348.1	0.7998	27.2		348.1	0.7998	25.1	
348.1	0.8998	30.1	64	348.2	0.9000	27.7	27

[a]Experimental uncertainty: T, ±0.1 K; P, ±0.0008 MPa; solubility, ±0.5 mol %; diffusivity, ±10%.

obtained at 283.2, 298.2, 323.2, and 348.2 K and pressures up to 0.9 MPa using a Hiden IGA microbalance. The experimental solubility results for HCFC-22 in [bmim][BF_4] and [bmim][PF_6] are tabulated in Table 3, while Table 4 lists the results for HCFC-22 in [emim][Tf_2N] and [emim][TFES]. As expected, the PTx data show that HCFC-22 solubility is directly proportional to pressure and inversely proportional to temperature. Figure 1 shows a comparison of HCFC-22 solubility in the four ILs at 298.2 K relative to Raoult's law. The measured solubility of HCFC-22 was greatest in [emim][Tf_2N], especially at low pressures (<0.5 MPa), where negative Raoult's law deviations were observed. Interestingly, the solubility values of HCFC-22 in [bmim][BF_4], [bmim][PF_6], and [emim][TFES] were nearly identical, <5 mol % deviation at all pressures. These three IL + HCFC-22 systems displayed Raoult's law behavior at pressures up to ∼0.5 MPa, and all four systems showed slightly positive Raoult's law deviations at higher pressures.

DOI: 10.1021/acs.iecr.9b02419
Ind. Eng. Chem. Res. 2019, 58, 11072−11081

Table 4. Experimental Solubility (PTx) and Diffusivity (D) Data for HCFC-22 in [emim][Tf_2N] and [emim][TFES]

(1) HCFC-22 + (2) [emim][Tf_2N]				(1) HCFC-22 + (2) [emim][TFES]			
T (K)	P (MPa)	mol % ($100x_1$)	$D \times 10^{-11}$ (m^2/s)	T (K)	P (MPa)	mol % ($100x_1$)	$D \times 10^{-11}$ (m^2/s)
283.1	0.0500	12.6	4.5	283.2	0.0498	8.6	1.7
283.2	0.1000	23.1		283.1	0.0996	16.8	
283.2	0.2000	40.1		283.2	0.2000	32.0	
283.2	0.3000	53.3	26	283.2	0.3000	46.0	6.6
283.2	0.4000	64.2		283.1	0.4000	58.5	
283.2	0.5000	73.7		283.2	0.5000	69.8	
283.1	0.6000	83.5	69	283.2	0.6000	81.0	42
298.2	0.0500	7.9	8.8	298.1	0.0500	5.2	3.1
298.2	0.1000	15.2		298.2	0.1000	10.4	
298.2	0.2000	27.8		298.1	0.2000	20.5	
298.2	0.3000	38.4	22	298.2	0.3000	30.0	6.8
298.2	0.4000	47.3		298.1	0.4000	39.1	
298.2	0.5000	55.1		298.2	0.5000	47.4	
298.2	0.6000	62.0	46	298.2	0.6000	55.3	19
298.2	0.7000	68.4		298.2	0.7000	62.8	
298.2	0.8000	74.5		298.2	0.8000	70.0	
298.2	0.8997	80.8	86	298.2	0.8999	77.3	47
298.2	0.8997	80.8		298.2	0.8999	77.3	
298.1	0.7994	74.5		298.2	0.7998	69.9	
298.2	0.7000	68.4		298.1	0.7000	62.7	
298.2	0.6000	62.0		298.2	0.6000	55.2	
298.2	0.5000	55.1		298.2	0.5000	47.4	
298.2	0.4000	47.4		298.2	0.4000	39.1	
298.1	0.3000	38.6		298.2	0.3000	30.2	
298.2	0.2000	28.1		298.2	0.2000	20.6	
298.2	0.1000	15.6		298.2	0.1000	10.5	
298.2	0.0500	8.2		298.2	0.0500	5.5	
323.2	0.0500	4.2	12	323.1	0.0500	2.9	5.1
323.2	0.1000	8.2		323.1	0.1000	5.7	
323.2	0.1999	15.6		323.2	0.2000	11.2	
323.2	0.3000	22.4	25	323.2	0.3000	16.5	9.9
323.2	0.4000	28.6		323.2	0.4000	21.5	
323.2	0.5000	34.2		323.2	0.5000	26.4	
323.1	0.5996	39.3	40	323.2	0.6000	31.1	14
323.2	0.6997	44.1		323.1	0.6998	35.6	
323.2	0.7996	48.4		323.2	0.7997	39.9	
323.2	0.9000	52.5	50	323.2	0.8998	44.3	23
348.1	0.0500	2.4	24	348.2	0.0500	1.6	12
348.1	0.1000	4.8		348.2	0.1000	3.2	
348.2	0.2000	9.5		348.1	0.2000	6.6	
348.2	0.3000	13.8	36	348.2	0.3000	9.9	18
348.2	0.4000	17.9		348.1	0.4000	13.1	
348.2	0.4996	21.8		348.1	0.5000	16.2	
348.2	0.5999	25.6	39	348.2	0.5998	19.2	18
348.2	0.6993	28.9		348.1	0.6997	22.1	
348.2	0.7993	32.3		348.2	0.7996	25.2	
348.2	0.8996	35.4	67	348.2	0.8999	27.9	21

[a]Experimental uncertainty: T, ±0.1 K; P, ±0.0008 MPa; solubility, ±0.5 mol %; diffusivity, ±10%.

Shiflett et al. previously measured the solubility of several fluorinated refrigerant gases including difluoromethane (CHF_2-H, R-32),[4] fluoroform (CHF_2-F, R-23),[27] (1,1-difluoroethane (CHF_2-CH_3, R-152a) (tabulated data shown in the Supporting Information), and pentafluoroethane (CHF_2-CF_3, R-125)[11] in [emim][Tf_2N]. The refrigerant gas solubility results are compared to those of chlorodifluoromethane (CHF_2-Cl) as a function of normalized pressure at 298.2 K, in Figure 2.

The results in Figure 2 show how the substituent functional group (R) attached to the CHF_2 molecule (e.g., CHF_2-R) impacts the solubility of the refrigerant gas in [emim][Tf_2N]. Importantly, the results in Figure 2 have been presented with the pressure of each gas normalized by its vapor pressure, thus removing bias due to the different saturation pressures of the gases. The highest solubilities are observed with the refrigerant gases that have increasingly polar (R) groups. For instance, the order of solubility is CHF_2-Cl > CHF_2-F > CHF_2-CH_3 >

DOI: 10.1021/acs.iecr.9b02419
Ind. Eng. Chem. Res. 2019, 58, 11072−11081

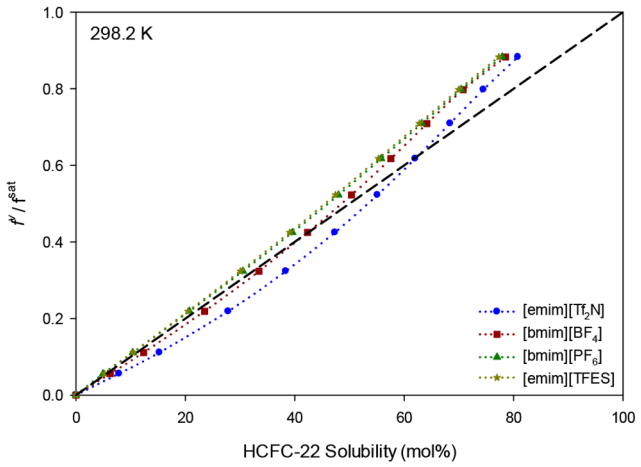

Figure 1. Solubility comparison of HCFC-22 in [emim][Tf_2N], [bmim][BF_4], [bmim][PF_6], and [emim][TFES] as a function of normalized fugacity at 298.2 K. Raoult's law shown using the black, long-dashed line.

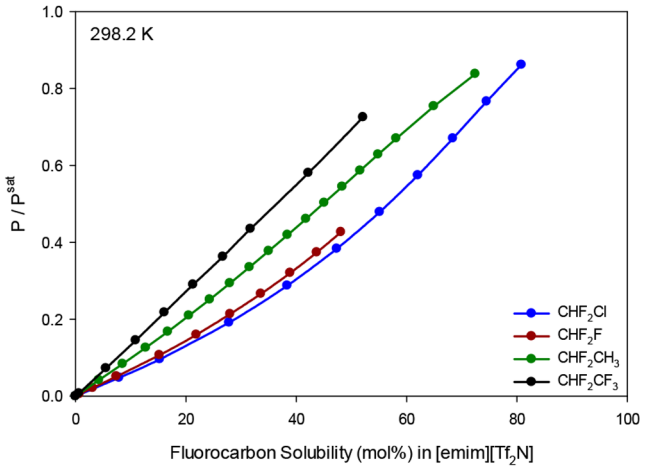

Figure 2. Solubility comparison of select fluorocarbon gases in [emim][Tf_2N] at 298.2 K as a function of normalized pressure.

CHF_2-CF_3. The theorized fluorocarbon absorption mechanism is driven by hydrogen bonding between the acidic hydrogen atom on the fluorocarbon molecule and an electronegative fluorine atom on the IL anion. By inspection of the results in Figure 2, it is evident that fluorocarbon molecules with polar, electronegative R groups have higher solubilities in ILs. Shiflett et al. previously investigated the fluorocarbon molecule dipole moment as a parameter that could influence solubility in an IL but found no correlation.[8] Molecular dynamics simulations, spectroscopic studies, and calorimetric investigations would add significant insight into the observed solubility trends.

Figures 3−6 show isothermal solubility results for HCFC-22 in [emim][Tf_2N], [bmim][BF_4], [bmim][PF_6], and [emim]-[TFES]. The figures plot the experimental data (symbols) with the temperature-dependent NRTL activity coefficient results (lines). The temperature-dependent binary interaction parameters for the NRTL activity coefficient model are shown in Table 5. Desorption data are also presented at 298.2 K (open squares) for each system in Figures 3−6. At 298.2 K, the absorption−desorption data points agreed to within ±0.2 mol % for the [emim][Tf_2N], [bmim][PF_6], and [emim][TFES] IL systems and to within ±1.0 mol % for [bmim][BF_4]. These

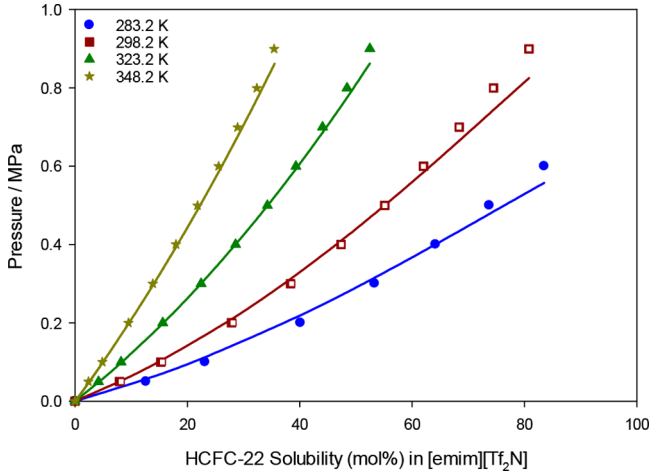

Figure 3. Isothermal $P-x$ solubility diagram for HCFC-22 in [emim][Tf_2N]. Closed symbols display absorption data and open squares display desorption data. Lines show NRTL model calculations.

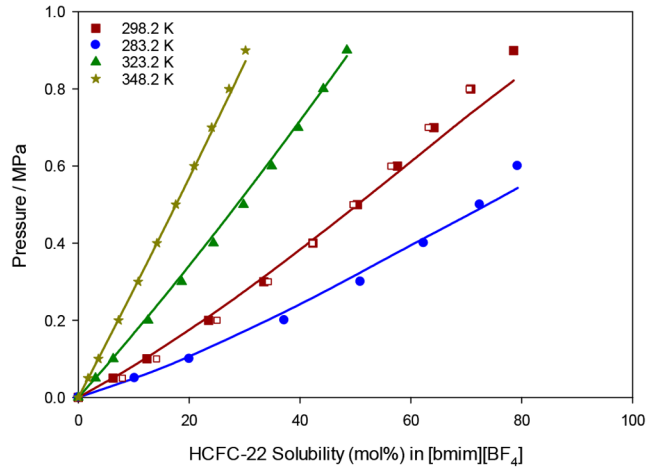

Figure 4. Isothermal $P-x$ solubility diagram for HCFC-22 in [bmim][BF_4]. Closed symbols display absorption data and open squares display desorption data. Lines show NRTL model calculations.

values are within the reported accuracy of the microbalance, i.e., ±0.5 mol %. Comparing the absorption/desorption results indicates that HCFC-22 desorption is rapid and that the IL−refrigerant gas interactions are most likely physical (non-chemical) in nature.

The solubility of HCFC-22 in each IL is linearly proportional to pressure, at pressures up to 0.2 MPa, and therefore obeys Raoult's law in the dilute regime. Henry's law constants were obtained using the methods shown in section 2.2.4, and the results are tabulated in Table 6. As expected, the Henry's law constant is directly proportional to temperature, indicating that HCFC-22 solubility is inversely proportional to T. Additionally, comparing the HCFC-22 Henry's law constants at 298.2 K for each IL shows that k_H (MPa) follows the order [emim][Tf_2N] < [bmim][BF_4] < [bmim][PF_6] ≈ [emim]-[TFES], which matches the general solubility trend displayed in Figure 2, where the greatest HCFC-22 solubility was measured in [emim][Tf_2N] with lesser amounts in the other ILs.

DOI: 10.1021/acs.iecr.9b02419
Ind. Eng. Chem. Res. 2019, 58, 11072−11081

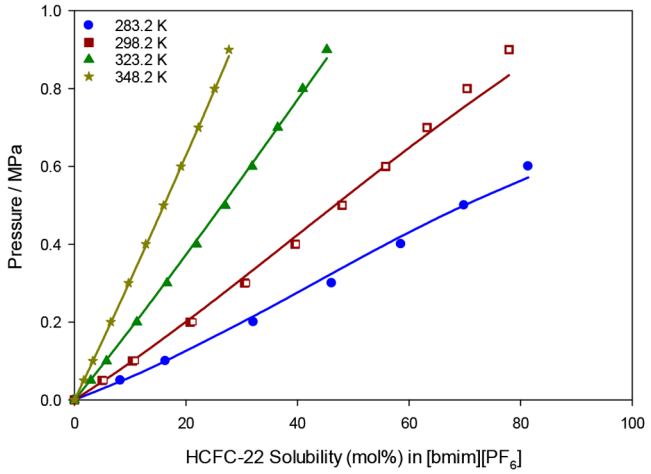

Figure 5. Isothermal $P-x$ solubility diagram for HCFC-22 in [bmim][PF_6]. Closed symbols display absorption data and open squares display desorption data. Lines show NRTL model calculations.

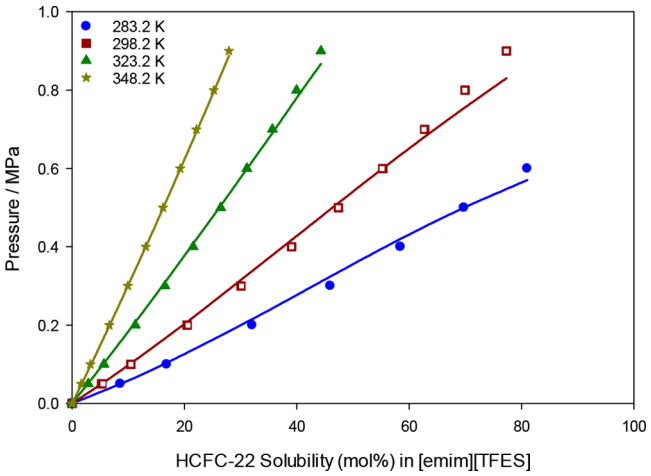

Figure 6. Isothermal $P-x$ solubility diagram for HCFC-22 in [emim][TFES]. Closed symbols display absorption data and open squares display desorption data. Lines show NRTL model calculations.

The enthalpy ($\Delta\bar{H}_{sol}$) and entropy ($\Delta\bar{S}_{sol}$) of absorption at infinite dilution were calculated using the van't Hoff relations shown in section 2.2.4. The results, shown in Table 7, indicate that HCFC-22 absorption is exothermic and enthalpically favorable but entropically unfavorable. Similar results have been observed in other fluorocarbon + IL systems.[9]

3.3. Diffusion Coefficient Results. The diffusivity of HCFC-22 was calculated for each IL system at each experimental temperature and pressures of ~0.05, 0.3, 0.6, and 0.9 MPa using a simplified Fickian diffusion model (see section 2.2.5). The diffusion coefficient results for HCFC-22 in each of the imidazolium ILs are tabulated in Tables 3 and 4 and are of a similar order of magnitude as those previously measured by Shiflett et al. for other refrigerant gas + IL systems ($D \approx 10^{-10}-10^{-11}$ m^2/s).[8] In general, the diffusivity of HCFC-22 increases exponentially with pressure, at a fixed temperature. For instance, at 298.2 K the diffusion coefficient of HCFC-22 in [emim][Tf_2N] is 8.8, 22, 46, and 86 × 10^{-11} m^2/s at pressures of 0.05, 0.3, 0.6, and 0.9 MPa. These represent increases of 150%, 423%, and 877%, respectively, relative to the diffusion coefficient at 0.05 MPa. As previously discussed, HCFC-22 solubility is directly proportional to pressure. By inspection it is evident that the absorption of HCFC-22 increases the free volume of the solution and concomitantly decreases the liquid-phase viscosity, resulting in the observed increase in the calculated diffusion coefficients. Analyzing the diffusion coefficient trend with respect to temperature, at a constant pressure, is complex, since multiple factors simultaneously affect the liquid-phase viscosity. For instance, the IL viscosity is inversely proportional to temperature. Therefore, all else being equal, higher temperatures would increase the transport properties of HCFC-22 in the liquid phase. However, HCFC-22 solubility is inversely proportional to temperature and, as was observed in the isothermal analysis, solubility has a significant effect on the diffusion coefficient. For these reasons, a simple qualitative trend cannot be made for the diffusion coefficient as a function of temperature at a fixed pressure.

The Stokes–Einstein relationship described in section 2.2.6 was used to calculate the molecular radius of the diffusing species (HCFC-22) in the liquid phase. The calculated Stokes–Einstein radii of the diffusing species in [bmim][BF_4], [emim][Tf_2N], [bmim][PF_6], and [emim][TFES] were 0.33, 0.58, 0.65, and 1.09 nm, respectively. The molecular radius of HCFC-22 was also calculated to be 0.35 nm using the Gaussian 09 software package with a MP2 method and the 6331-G(d,p) basis set. The Gaussian 09 calculated radius of

Table 6. HCFC-22 Henry's Law Constants (k_H, MPa)

ionic liquid	283.2 K	298.2 K	313.2 K	348.2 K
[emim][Tf_2N]	0.34 ± 0.02	0.55 ± 0.02	1.08 ± 0.01	1.94 ± 0.01
[bmim][BF_4]	0.36 ± 0.04	0.77 ± 0.03	1.45 ± 0.02	2.67 ± 0.01
[bmim][PF_6]	0.56 ± 0.01	0.90 ± 0.01	1.70 ± 0.01	3.00 ± 0.04
[emim][TFES]	0.56 ± 0.01	0.92 ± 0.01	1.72 ± 0.01	2.92 ± 0.02

Table 7. Enthalpy and Entropy of Absorption of HCFC-22 at Infinite Dilution

ionic liquid	$\Delta\bar{H}_{sol}$ (kJ/mol)	$\Delta\bar{S}_{sol}$ (J/mol·K)
[emim][Tf_2N]	−22.0 ± 0.16	−70.1 ± 1.83
[bmim][BF_4]	−24.5 ± 2.10	−77.9 ± 7.93
[bmim][PF_6]	−21.0 ± 0.17	−67.1 ± 1.58
[emim][TFES]	−20.6 ± 0.45	−65.7 ± 2.70

Table 5. Binary Interaction Parameters for the NRTL Activity Coefficient Model

system [HCFC-22 (1) + IL (2)]	$\tau_{12}^{(0)}$	$\tau_{12}^{(1)}$ (K)	$\tau_{12}^{(2)}$ [ln(K)$^{-1}$]	$\tau_{21}^{(0)}$	$\tau_{21}^{(1)}$ (K)	$\tau_{21}^{(2)}$ [ln(K)$^{-1}$]	error [%AARD (P)]
[emim][Tf_2N]	560.33	−25028.87	−83.13	−294.96	12978.63	43.78	3.5
[bmim][BF_4]	−16.54	2880.07	1.66	−25.49	−216.42	4.31	3.3
[bmim][PF_6]	−529.37	26061.66	78.04	166.10	−8616.34	−24.35	2.7
[emim][TFES]	−642.90	31153.20	94.96	238.35	−11875.24	−35.10	2.8

DOI: 10.1021/acs.iecr.9b02419
Ind. Eng. Chem. Res. 2019, 58, 11072–11081

HCFC-22 is similar to prior calculations conducted by Yokozeki et al., who estimated the molecular radii of difluoromethane (HFC-32) and fluoroform (HFC-23) to be 0.17 nm.[28] The chlorine (R) group on HCFC-22 (CHF_2-Cl) is larger than both hydrogen on HFC-32 (CHF_2-H) and fluorine on HFC-23 (CHF_2-F), which potentially explains the observed results.

In this study, the calculated Stokes−Einstein radius of HCFC-22 varied significantly, depending on the IL sorbent phase. Shiflett et al. previously hypothesized that fluorocarbon molecules could be diffusing in ILs as clusters or molecular associations.[4] These results indicate that HCFC-22 may diffuse as a single species in [bmim][BF_4] (r = 0.33 nm), while clusters of two HCFC-22 molecules may diffuse in [bmim][PF_6] (r = 0.65 nm) and [emim][Tf_2N] (r = 0.58 nm), with larger clusters of three molecules diffusing in [emim][TFES] (r = 1.09 nm). On the basis of the observed results, it is hypothesized that interactions between the fluorocarbon solute and the IL anion may influence the clustering effect and radius of the diffusing species. Spectroscopic experiments and molecular dynamic simulations could provide further insight into this hypothesis.

4. CONCLUSION

The solubility and diffusivity of chlorodifluoromethane (HCFC-22) was measured in [emim][Tf_2N], [bmim][BF_4], [bmim][PF_6], and [emim][TFES] using a Hiden IGA gravimetric microbalance. Measurements were obtained at temperatures of 283.2, 298.2, 323.2, and 348.2 K and at pressures ranging from 0.05 to 0.9 MPa. The solubility results were modeled using a $\gamma-\phi$ method where the liquid phase was modeled using the NRTL activity coefficient method and the vapor phase was modeled by a second virial coefficient correction. The NRTL model provided a good fit of the experimental data with an average deviation in pressure of less than 4% AARD. Infinite dilution Henry's law constants were calculated from the *PTx* results and were used to calculate the enthalpy and entropy of absorption of HCFC-22 in each of the ionic liquids. The results demonstrated that HCFC-22 absorption is enthalpically favorable ($-\Delta\bar{H}_{sol}$) and entropically unfavorable ($-\Delta\bar{S}_{sol}$). Diffusivity results for HCFC-22 were calculated using the time-dependent absorption data generated by the microbalance and were on the order of $10^{-10}-10^{-11}$ m^2/s and were dependent on the experimental temperature, pressure, and ionic liquid. Finally, the Stokes−Einstein equation was used to calculate the effective radius of the diffusing species. The results showed that the diffusing radius of HCFC-22 was 0.33 nm in [bmim][BF_4], 0.58 nm in [emim][Tf_2N], 0.65 nm in [bmim][PF_6], and 1.09 nm in [emim][TFES]. The results seem to suggest that HCFC-22 molecules could be diffusing as a single species in [bmim][BF_4] and as clusters in [bmim][PF_6], [emim][Tf_2N], and [emim][TFES].

■ ASSOCIATED CONTENT

Supporting Information

The Supporting Information is available free of charge on the ACS Publications website at DOI: 10.1021/acs.iecr.9b02419.

Table S1: Experimental solubility (*PTx*) data for HFC-152a in [emim][Tf_2N] (PDF)

■ AUTHOR INFORMATION

Corresponding Author

*Phone: +1 (785) 864-4947. Fax: +1 (785) 864-4967. E-mail: mark.b.shiflett@ku.edu.

ORCID

David L. Minnick: 0000-0001-7733-7371

Mark B. Shiflett: 0000-0002-8934-6192

Present Address

†D.L.M.: DuPont, 8480 DuPont Rd., Parkersburg, WV 26101.

Author Contributions

All authors contributed equally.

Notes

The authors declare no competing financial interest.

■ ACKNOWLEDGMENTS

The authors would like to acknowledge Tugba Turnaoglu for her assistance with developing the MATLAB code used to perform the diffusion coefficient modeling. The authors would also like to acknowledge Luke D. Simoni (Chemours) for his assistance with calculating the HCFC-22 molecular radius using the Gaussian 09 software package. This research received no external funding support.

■ REFERENCES

(1) Abas, N.; Kalair, A. R.; Khan, N.; Haider, A.; Saleem, Z.; Saleem, M. S. Natural and synthetic refrigerants, global warming: A review. *Renewable Sustainable Energy Rev.* **2018**, *90*, 557−569.

(2) Shiflett, M. B.; Yokozeki, A. Utilizing ionic liquids for hydrofluorocarbon separation. US patent 8,628,644, 2006.

(3) Shiflett, M. B.; Corbin, D. R.; Elliott, B. A.; Yokozeki, A. Sorption of trifluoromethane in zeolites and ionic liquid. *J. Chem. Thermodyn.* **2013**, *64*, 40−49.

(4) Shiflett, M. B.; Harmer, M. A.; Junk, C. P.; Yokozeki, A. Solubility and diffusivity of difluoromethane in room-temperature ionic liquids. *J. Chem. Eng. Data* **2006**, *51* (2), 483−495.

(5) Shiflett, M. B.; Harmer, M. A.; Junk, C. R.; Yokozeki, A. Solubility and diffusivity of 1,1,1,2-tetrafluoroethane in room-temperature ionic liquids. *Fluid Phase Equilib.* **2006**, *242* (2), 220−232.

(6) Shiflett, M. B.; Maginn, E. J. The Solubility of Gases in Ionic Liquids. *AIChE J.* **2017**, *63* (11), 4722−4737.

(7) Shiflett, M. B.; Yokozeki, A. Solubilities and diffusivities of carbon dioxide in ionic liquids: [bmim][PF6] and [bmim][BF4]. *Ind. Eng. Chem. Res.* **2005**, *44* (12), 4453−4464.

(8) Shiflett, M. B.; Yokozeki, A. Solubility and diffusivity of hydrofluorocarbons in room-temperature ionic liquids. *AIChE J.* **2006**, *52* (3), 1205−1219.

(9) Shiflett, M. B.; Yokozeki, A. Gaseous absorption of fluoromethane, fluoroethane, and 1,1,2,2-tetrafluoroethane in 1-butyl-3-methylimidazolium hexafluorophosphate. *Ind. Eng. Chem. Res.* **2006**, *45* (18), 6375−6382.

(10) Shiflett, M. B.; Yokozeki, A. Solubility differences of halocarbon isomers in ionic liquid [emim][Tf2N]. *J. Chem. Eng. Data* **2007**, *52* (5), 2007−2015.

(11) Shiflett, M. B.; Yokozeki, A. Binary Vapor−Liquid and Vapor−Liquid−Liquid Equilibria of Hydrofluorocarbons (HFC-125 and HFC-143a) and Hydrofluoroethers (HFE-125 and HFE-143a) with Ionic Liquid [emim][Tf2N]. *J. Chem. Eng. Data* **2008**, *53* (2), 492−497.

(12) Shiflett, M. B.; Yokozeki, A. Separation of difluoromethane and pentafluoroethane by extractive distillation using ionic liquid. *Chimica Oggi* **2006**, *24* (2), 28−30.

(13) Shiflett, M. B.; Yokozeki, A. Process for purifying perfluorinated products. US Patent 8,771,626, 2007.

(14) Minnick, D. L.; Turnaoglu, T.; Rocha, M. A.; Shiflett, M. B. Review Article: Gas and vapor sorption measurements using electronic beam balances. *J. Vac. Sci. Technol., A* **2018**, *36* (5), 050801.
(15) Lemmon, E. W. H., M. L; Mclinden, M. O. *REFPROP 9.1*, NIST Reference Fluid Thermodynamic and Transport Properties Database; NIST, 2013.
(16) Fröba, A. P.; Kremer, H.; Leipertz, A. Density, Refractive Index, Interfacial Tension, and Viscosity of Ionic Liquids [EMIM][EtSO4], [EMIM][NTf2], [EMIM][N(CN)2], and [OMA][NTf2] in Dependence on Temperature at Atmospheric Pressure. *J. Phys. Chem. B* **2008**, *112* (39), 12420−12430.
(17) Neves, C. M. S. S.; Kurnia, K. A.; Coutinho, J. A. P.; Marrucho, I. M.; Lopes, J. N. C.; Freire, M. G.; Rebelo, L. P. N. Systematic Study of the Thermophysical Properties of Imidazolium-Based Ionic Liquids with Cyano-Functionalized Anions. *J. Phys. Chem. B* **2013**, *117* (35), 10271−10283.
(18) Salgado, J.; Regueira, T.; Lugo, L.; Vijande, J.; Fernández, J.; García, J. Density and viscosity of three (2,2,2-trifluoroethanol+1-butyl-3-methylimidazolium) ionic liquid binary systems. *J. Chem. Thermodyn.* **2014**, *70*, 101−110.
(19) Larriba, M.; García, S.; García, J.; Torrecilla, J. S.; Rodríguez, F. Thermophysical Properties of 1-Ethyl-3-methylimidazolium 1,1,2,2-Tetrafluoroethanesulfonate and 1-Ethyl-3-methylimidazolium Ethylsulfate Ionic Liquids as a Function of Temperature. *J. Chem. Eng. Data* **2011**, *56* (9), 3589−3597.
(20) Neilson, E. F.; White, D. The heat capacity, heat of fusion, heat of transition and heat of vaporization of chlorodifluoromethane between 16 K and the boiling point. *J. Am. Chem. Soc.* **1957**, *79*, 5618−5621.
(21) Kamei, A.; Beyerlein, S. W.; Jacobsen, R. T. Application of nonlinear regression in the development of a wide range formulation for HCFC-22. *Int. J. Thermophys.* **1995**, *16* (5), 1155−1164.
(22) Yokozeki, A. Solubility and viscosity of refrigerant−oil mixtures. *International Compressor Engineering Conference*; 1994; paper 1002.
(23) Thermodynamics of Ionic Liquids, Ionic Liquid Mixtures, and the Development of Standardized Test Systems. https://www.iupac.org/publications/ci/2005/2705/pp4_2002-005-1-100.html.
(24) Gomes, M. F. C. Low-pressure solubility and thermodynamics of solvation of carbon dioxide, ethane, and hydrogen in 1-hexyl-3-methylimidazolium bis(trifluoromethylsulfonyl)amide between temperatures of 283 and 343 K. *J. Chem. Eng. Data* **2007**, *52* (2), 472−475.
(25) Kumelan, J.; Pérez-Salado Kamps, I. P. S.; Tuma, D.; Maurer, G. Solubility of CO2 in the ionic liquid [hmim][Tf2N]. *J. Chem. Thermodyn.* **2006**, *38* (11), 1396−1401.
(26) Shiflett, M. B.; Yokozeki, A. Solubility of CO2 in room temperature ionic liquid [hmim][Tf2N]. *J. Phys. Chem. B* **2007**, *111* (8), 2070−2074.
(27) Shiflett, M. B.; Corbin, D. R.; Yokozeki, A. Comparison of the Sorption of Trifluoromethane (R-23) on Zeolites and in an Ionic Liquid. *Adsorpt. Sci. Technol.* **2013**, *31* (1), 59−83.
(28) Yokozeki, A.; Sato, H.; Watanabe, K. Ideal-gas heat capacities and virial coefficients of HFC refrigerants. *Int. J. Thermophys.* **1998**, *19* (1), 89−127.

DOI: 10.1021/acs.iecr.9b02419
Ind. Eng. Chem. Res. 2019, 58, 11072−11081